Analog Gradient Beamformer for a Wireless Ultrasound Scanner.

di Ianni, Tommaso; Hemmsen, Martin Christian; Bagge, Jan Peter; Jensen, Henrik; Vardi, Nitsan; Jensen, Jørgen Arendt

Published in:
Proceedings of SPIE

Link to article, DOI:
10.1117/12.2216238

Publication date:
2016

Document Version
Peer reviewed version

Analog Gradient Beamformer for a Wireless Ultrasound Scanner

Tommaso Di Ianni[a], Martin Christian Hemmsen[a], Jan Bagge[b], Henrik Jensen[b], Nitsan Vardi[b], Jørgen Arendt Jensen[a]

[a]Center for Fast Ultrasound Imaging, Department of Electrical Engineering, Technical University of Denmark, DK-2800 Lyngby, Denmark
[b]BK Ultrasound, DK-2730 Herlev, Denmark

ABSTRACT

This paper presents a novel beamformer architecture for a low-cost receiver front-end, and investigates if the image quality can be maintained. The system is oriented to the development of a hand-held wireless ultrasound probe based on Synthetic Aperture Sequential Beamforming, and has the advantage of effectively reducing circuit complexity and power dissipation. The array of transducers is divided into sub-apertures, in which the signals from the single channels are aligned through a network of cascaded gradient delays, and summed in the analog domain before A/D conversion. The delay values are quantized to simplify the shifting unit, and a single A/D converter is needed for each sub-aperture yielding a compact, low-power architecture that can be integrated in a single chip. A simulation study was performed using a 3.75 MHz convex array, and the point spread function (PSF) for different configurations was evaluated in terms of lateral full-width-at-half-maximum (FWHM) and -20 dB cystic resolution (CR). Several setups were simulated varying the sub-aperture size N and the quantization step, and design constraints were obtained comparing the PSF to that of an ideal non-quantized system. The PSF is shown for $N = 32$ with a quantization step of 12 ns. For this configuration, the FWHM is degraded by 0.25% and the CR is 8.70% lower compared to the ideal situation. The results demonstrate that the gradient beamformer provides an adequate image quality, and open the way to a fully-integrated chip for a compact, low-cost, wireless ultrasound probe.

Keywords: analog beamformer, portable scanner, Synthetic Aperture Sequential Beamforming, point-of-care ultrasound

1. INTRODUCTION

The use of portable ultrasound for point-of-care examinations in non-conventional setups has attracted increasing interest among the medical community. Hand-held devices have the potential to bring ultrasound imaging out of the hospital setting and improve the access to healthcare in developing countries.[1,2] The development of a battery-powered low-weight scanner brings about new requirements in terms of power consumption, cost and flexibility. On the other hand, a proper image quality needs to be maintained to preserve the clinical functionality of the device.

The first challenge in the design of a wireless system is represented by the minimization of the data transfer rate between the probe and the processing unit. In a conventional digital dynamic receive beamformer, 208 µs need to be transferred per emission for each of the active receiving elements, if a depth of 16 cm is to be visualized. For a $M = 64$ channels aperture, for instance, with a sampling frequency $f_s = 30$ MHz, the data throughput is $208\,\mu\text{s} \times f_s M \sim 400$k samples per emission.

A number of different approaches in the last decades have addressed the relaxation of the data throughput requirement. Poland *et al.*[3] presented a low-weight wireless solution based on micro-beamforming.[4–6] The method lightens the burden of interconnection between the probe and the central unit moving part of the

Send correspondence to: Tommaso Di Ianni, E-mail: todiian@elektro.dtu.dk

beamformation in the transducer handle. K elements are grouped together in a sub-aperture that is pre-beamformed before transmission, thus the transfer rate is reduced by a factor of K. For a sub-aperture size $K = 8$, for example, $208\,\mu s \times f_s M/K \sim 50$k samples are transferred per emission.

A wireless ultrasound scanner was also commercialized by Siemens Medical Solutions USA, Inc.[7] However, the system uses proprietary protocols for the radio communication, and therefore dedicated circuitry needs to be used. The cost of the system may be drastically lowered by using commercial general-purpose components.

Hemmsen *et al.*[8,9] demonstrated the feasibility of B-mode and blood flow imaging using commercial mobile devices such as tablets and smartphones. These are wirelessly connected to an external probe for the acquisition of the ultrasound data, that is pre-beamformed in the transducer handle to minimize the data throughput. The system is based on Synthetic Aperture Sequential Beamforming (SASB).[10] The approach has been demonstrated in the clinic to provide images equally good compared to conventional dynamic receive focusing,[11] while reducing the system requirements due to the implementation of a static-focus beamformer in the transducer handle. Only a single beamformed line per emission needs to be transmitted to the central unit, and the transfer rate is reduced by a factor M. Referring to the previous example, the transfer rate is equal to $208\,\mu s \times f_s \sim 6$k samples per emission.

In this paper, a novel delay-and-sum beamformer oriented to the development of a SASB wireless probe is described. The array of transducers is divided into sub-apertures, and for each receive channel the delay value is integrated in successive steps through a series of cascaded all-pass filters. The signals from the sub-apertures are summed together before A/D conversion, and therefore a single A/D converter (ADC) is needed for each sub-aperture. In addition, the actual delay gradients are quantized to further reduce the circuit complexity, yielding a low-power architecture that can be integrated in a single chip. A simulation study was carried out with a 3.75 MHz convex array to evaluate the image quality and obtain operative design specifications based on a compromise between system complexity and image degradation.

The beamformer architecture and the simulation setup are described in Section 2, and the results presented in Section 3. Finally, Section 4 discusses the conclusions to the study.

2. METHODS

2.1 Synthetic Aperture Sequential Beamforming

SASB takes advantage of the improved image quality of Synthetic Aperture (SA) imaging without the need for computing and transferring a complete set of low-resolution frames.[10] The method has been clinically demonstrated to be equally good compared to conventional dynamic receive focusing,[11] with the advantages of reduced system requirements and effective reduction of the data transfer rate between the probe and the processing unit. A virtual source (VS) is emulated in front of the transducer by means of a focused emission. For each k-th emission, a single RF line $\ell_k(t)$ is beamformed in receive using a static focus located in the VS position. The beamformed RF lines are referred to as low-resolution lines in the remaining of the article.

The round trip time-of-flight for the first stage beamformer is calculated based on the propagation path shown in Fig. 1a, and is equal to

$$t_{fs}(\vec{r}_{ip}, k, j) = \frac{1}{c}(z_{pf_k} \pm |\vec{r}_{ip} - \vec{r}_{fp_k}| \pm |\vec{r}_{fp_k} - \vec{r}_{ip}| + |\vec{r}_{r_j} - \vec{r}_{fp_k}|). \tag{1}$$

In Eq. (1), $z_{pf_k} = |\vec{r}_{fp_k} - \vec{r}_{e_k}|$ is the distance from the focus point $\vec{r}_{fp_k}$ to the center of the aperture $\vec{r}_{e_k}$, $\vec{r}_{ip}$ is the image point, and $\vec{r}_{r_j}$ is the position of the $j-$th receiving transducer in the active aperture of M elements, with $j = 1, ..., M$. The $\pm$ in (1) refers to whether the image point is above or below the VS. The time-of-flight t_{fs} is therefore dependent on the image point, the emission index, and the receiving element.

In the second stage, a high-resolution image is obtained by re-focusing a number of low-resolution lines. The beamformed signals ℓ_k are considered as the responses of the virtual elements emitting/receiving spherical waves that propagate in a region spatially confined by the angle $\alpha = 2\arctan(1/2F\#)$. $F\#$ is the F-number equal to z_{fp}/L_A, where L_A is the aperture width. The sample for the image point $\vec{r}_{ip}$ is found in the k-th low-resolution line at the time

$$t_{ss}(\vec{r}_{ip}, k) = \frac{2}{c}(z_{pf} \pm |\vec{r}_{ip} - \vec{r}_{fp_k}|). \tag{2}$$

Again, the ± in (2) refers to the position of the image point relative to that of the VS. The time of flight t_{ss} is used in the second stage for the re-focusing of the low-resolution lines. For further details on the second stage beamformer, readers are referred to the cited articles on SASB.

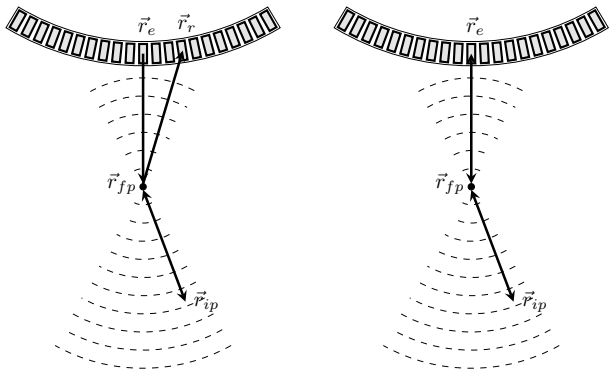

(a) (b)

Figure 1. Wave propagation path for the first stage (a) and second stage (b) beamformers. $\vec{r}_e$ and $\vec{r}_r$ are the emission reference point and the receiving element position, respectively; $\vec{r}_{fp}$ is the static focal position (virtual source); and $\vec{r}_{ip}$ is the image point.

2.2 Analog gradient beamformer

The core idea of gradient beamforming is illustrated in Fig. 2a. The array of transducer elements is divided into sub-apertures Σ_N of N receiving channels. The received signals are fed to a cascade of analog amplifiers for time-gain compensation and apodization, and pre-beamformed in the analog domain before A/D conversion. A coarse group delay T_g is then applied to the sub-aperture signal in the digital domain, and the digital sub-aperture signals are finally summed together before the transmission to the central processing unit, where the high-resolution images are attained by the second stage beamformer.

For each $k-$th emission, the delay value for the i-th channel is equal to $t_{fs}(k,i) = T_g + t_i$, with t_i the channel-dependent fine delay. Here $i = 1, ..., N$ is the channel index internal to the sub-aperture. The fine delays t_i are integrated in N-i+1 successive steps, as illustrated in Fig. 3, and are calculated as:

$$t_i = t_{fs}(k,i) - T_g = \nabla t_i + \nabla t_{i+1} + \cdots + \nabla t_N, \tag{3}$$

where ∇t_i is the difference between the delay values of the i-th and $(i+1)$-th channels. These values will be referred to as delay gradients in the remaining of the article. The fine delays are realized in the analog domain through a network of phase shifting all-pass filters, and the sum is calculated by the analog summer before the next delay is applied. To further simplify the architecture, only a discrete set of fine delay values can be considered, and these are assumed to be multiples of a the quantization step δt, as shown in Fig. 2b. This translates to the actual implementation by using a variable-length bank of elemental delay networks, cascaded to round the gradient ∇t_i to the nearest possible value. The coarse delay T_g is applied in the digital domain, and can be implemented by merely shifting the samples, if a sampling frequency adequately high is used, or by interpolating inter-sample values.

As a consequence of the grouping and quantization, the receiving channels experience dissimilar delay errors, and artefacts appear in the high-resolution images. For instance, the delay t_1 relative to the signal to be delayed the most (left edge in Fig. 3) is integrated through N gradients, each of which is quantized. The design of the proper sub-aperture size N and the quantization step size δt is of great importance to minimize the number of ADC's and the complexity of the delaying network while maintaining an adequate image quality.

The advantage of the gradient beamformer is the use of a single ADC for each sub-aperture Σ_N, and this effectively reduces the system complexity, power consumption and cost. Furthermore, the analog delaying function can be implemented with a compact RC network, and enables the possibility for the whole system to be

integrated in a single chip. This architecture differs from a micro-beamformer in the way that only a static focus is considered in receive, and a dynamic focus is obtained in the second stage beamformer.[4,5] The fine delay profile is therefore updated for every emission, and maintained for the whole duration of the receive event. Conversely, in a micro-beamformer the fine delays must be continuously updated during reception, and this complicates the sub-aperture processing, even if strong approximations such as linearization are considered.[6]

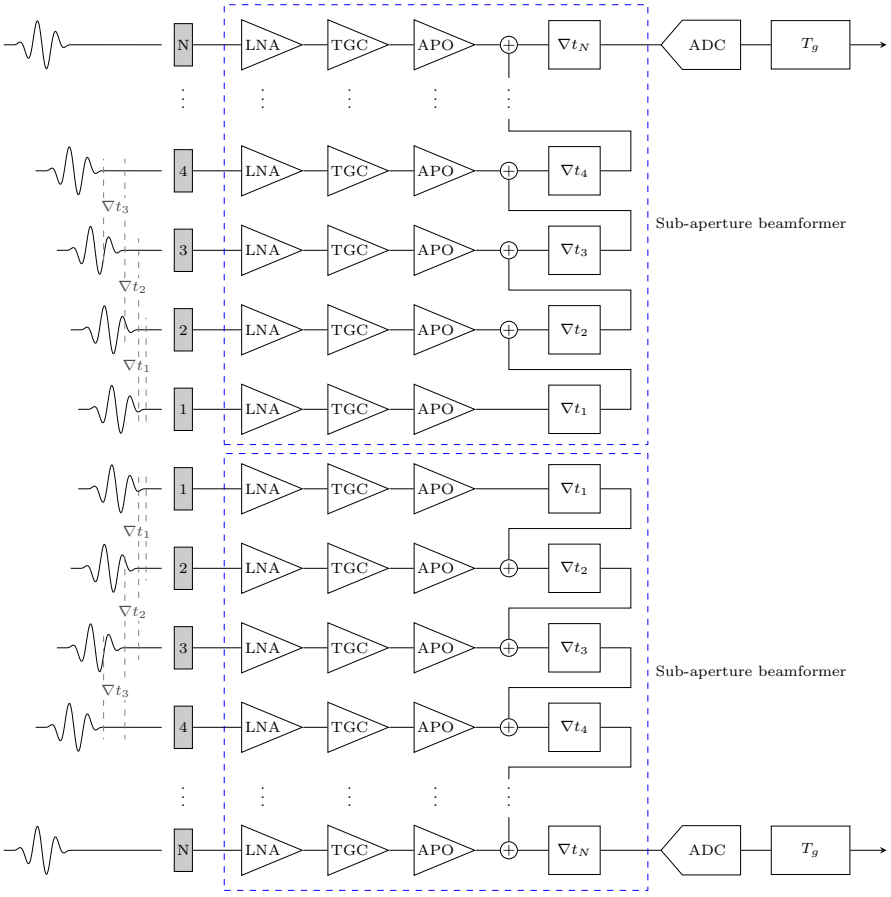

(a)

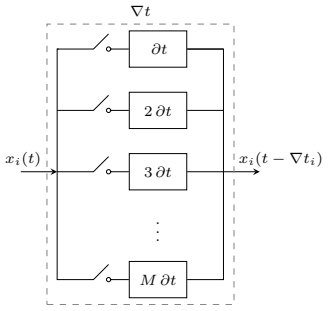

(b)

Figure 2. Schematic representation of the gradient delay beamformer system (a); conceptual implementation of the fine delay component (b).

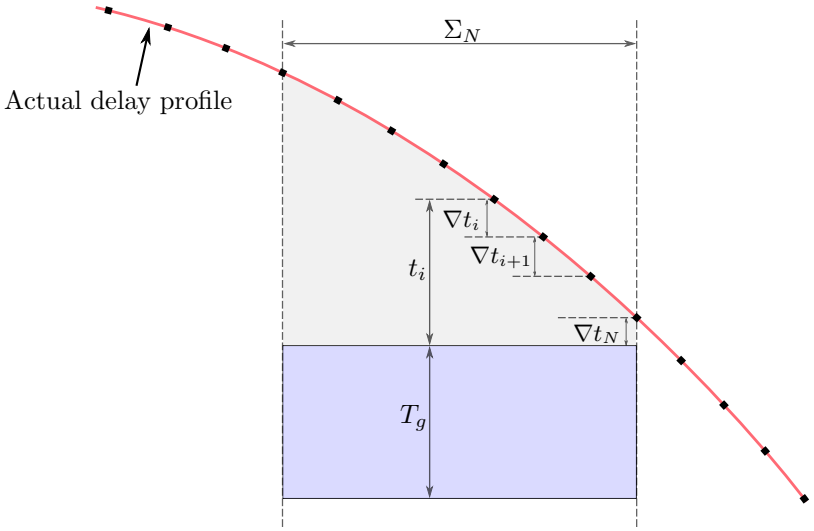

Figure 3. Gradient beamforming delay profile integration.

2.3 Simulation setup

A simulation study was performed in Field II[12,13] to evaluate the image degradation as a function of the sub-aperture size N and the quantization step size δt. Only the effect of the delay error was taken into account in the study, and other sources of image degradation were neglected. The point spread function (PSF) was simulated using a 3.75 MHz 192-element convex array transducer in a range from 10 to 130 mm in steps of 10 mm, with a fixed transmit/receive focus in 70 mm. The quantization step size was swept from 2 to 50 ns in steps of 2 ns, for $N = 2, 4, 8, 16, 32$. A sampling frequency of 60 MHz was considered for the calculation of the group delay T_g. The parameters of the simulation setup are reported in Table 1. A model of the gradient beamformer was developed in MATLAB (The MathWorks Inc., Natick, MA), and the second stage beamformer was implemented using BFT3 toolbox.[14] The high-resolution images were log-compressed after envelope detection, and finally visualized with a 60 dB dynamic range. The image quality was evaluated in terms of lateral full-width-at-half-maximum (FWHM) and −20 dB cystic resolution (CR),[15] defined as the radius ρ of a circular void centered on the PSF and providing a contrast

$$C(\rho) = 10 \log_{10} \left(1 - \frac{E_{in}(\rho)}{E_{tot}} \right) \tag{4}$$

equal to −20 dB. E_{in} and E_{tot} in Eq. (4) are the PSF energy inside the void and the total PSF energy. FWHM and CR were averaged over the simulated points and compared to the ideal non-quantized setup.

3. RESULTS

The average FWHM is shown in Fig. 4a. The resolution is close to the ideal value for quantization steps lower than 26 ns, with losses limited to 3.2% respect to the reference. A common trend is found for all the sub-aperture sizes considered in the simulation. For greater quantization steps, the resolution deteriorates and the FWHM increases with different slopes for different values of N.

As expected, the contrast is mostly affected by the delay errors even for limited quantization steps, as highlighted by the −20 dB CR in Fig. 4b. Small errors in the beamformation introduced by the quantization of the delays enhance the sidelobes level, degrading the PSF. The CR values for all the curves are close to the reference for steps smaller than 12 ns. This point provides an upper bound to the quantization step if the image quality of the ideal beamformer is to be maintained.

In Fig. 5 the PSF in 20 mm, 70 mm, and 120 mm is shown in the left and right column for the ideal non-quantized beamformer, and is compared to the one obtained using the gradient architecture with $N = 32$ and δt =12 ns in the right column. The visualized depths are chosen with the intention of showing the behaviour in the

Table 1. Simulation parameters

Transducer parameters	
Transducer	Convex array
Center frequency - f_0	3.75 MHz
Number of elements	192
Transducer element pitch	0.33 mm
Transducer element height	13 mm
Convex curvature radius	61 mm
Elevation focus	65 mm
Transmit parameters	
Excitation	2-cycle weighted sinusoid
Apodization function	Rect function
Active aperture size - M	64 elements
Virtual sources axial position	70 mm
$f\#$	3.3
Number of emissions	269
Receive parameters	
Apodization function	Hamming
Active aperture size - M	64 elements
Virtual sources axial position	70 mm
$f\#$	3.3
Second stage parameters	
Second stage apodization	Hamming

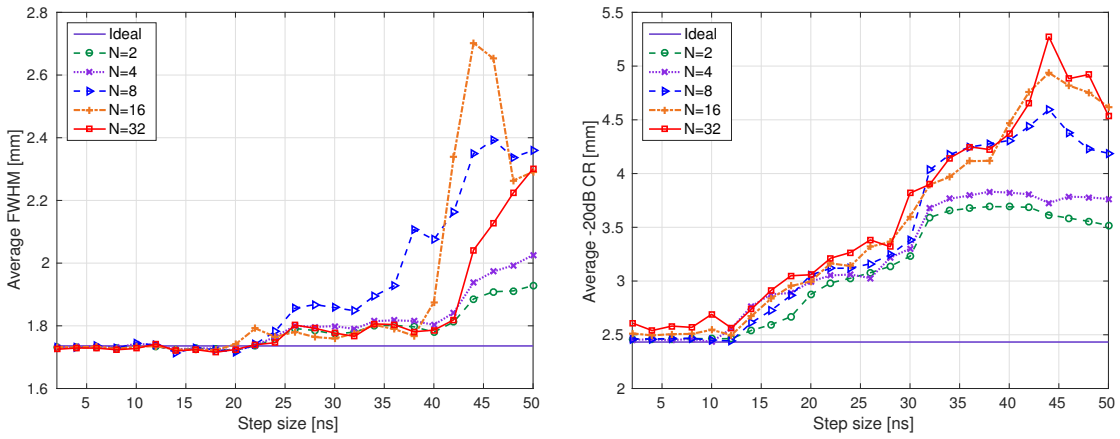

(a) (b)

Figure 4. Average FWHM (a) and -20 dB CR (b) as a function of the quantization step size for the PSF obtained with the gradient beamformer approach using sub-aperture sizes $N = 2, 4, 8, 16, 32$ and compared to the ideal setup.

near field, focal position, and far field. While the PSFs in 70 mm, and 120 mm show minimum degradation, the effect of the beamformation errors is clearly visible in the close field. In particular, the contrast is compromised as the sidelobes show higher spatial extension as well as higher intensity. For this setup, losses in average FWHM are limited to 0.25% and the average CR results degraded by less then 8.70%. It must be noted that for the setup with sub-aperture size $N = 32$, only two ADC are used for a 64-element active aperture.

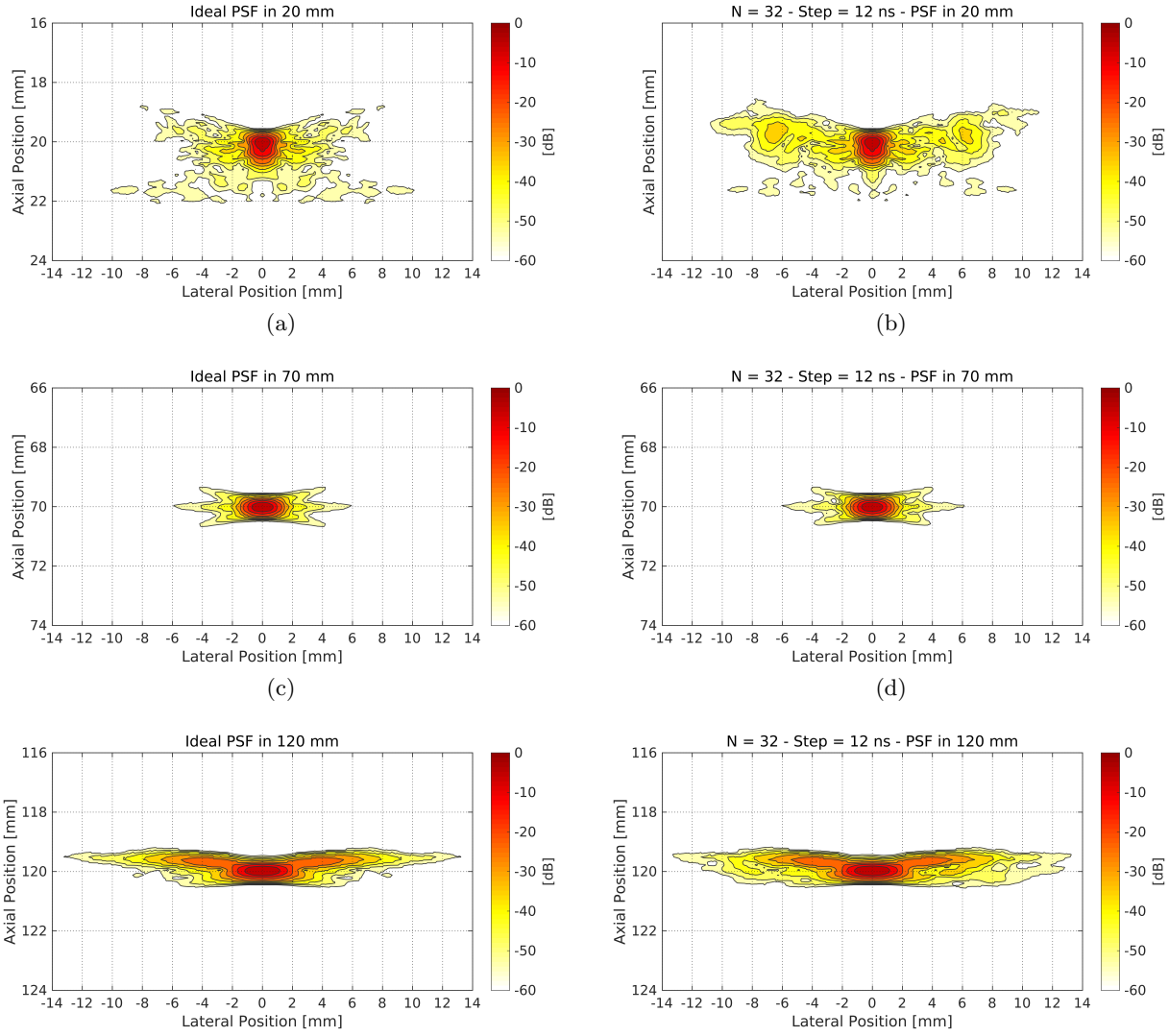

Figure 5. Simulated point spread function for the ideal beamformer (left column) and gradient beamformer with $N = 32, \delta t = 12$ ns (right column) in 20 mm (a,b); 70 mm (c,d); and 120 mm with a 3.75 MHz convex array transducer.

4. CONCLUSION

A novel analog beamformer architecture for the implementation of a low-cost wireless probe based on Synthetic Aperture Sequential Beamforming was presented and investigated in this study. The approach is based on the integration of the delay values through a series of all-pass shifting networks, and makes use of a single ADC for each sub-aperture. The actual gradient values are quantized to further reduce the system complexity, yielding a compact architecture that can be integrated in a single chip. The quantization introduces element-dependent errors in the beamformation which degrades the resolution and contrast of the imaging system. A simulation study was performed with a 3.75 MHz convex array to evaluate the image quality and obtain design constraints based on a comparison with an ideal non-quantized situation. The results show that a quantization step lower than 12 ns must be used to maintain approximately the same image quality as the ideal situation. The PSF was shown for the gradient beamformer with sub-aperture size $N = 32$ to evaluate the image degradation due to the delay errors. It turns out that the image quality is compromised in the near field, in particular for what concerns the contrast, as the sidelobes show higher intensity and spatial extension. For this configuration,

however, only two ADCs are needed for the whole active aperture. The results demonstrate that the analog gradient architecture is a suitable option for the development of a low-cost, low-power ultrasound wireless probe.

5. ACKNOWLEDGEMENTS

This work was supported by grant 82-2012-4 from the Danish National Advanced Technology Foundation and by BK Ultrasound, Herlev, Denmark.

REFERENCES

[1] Mehta, M., Jacobson, T., Peters, D., Le, E., Chadderdon, S., Allen, A. J., Caughey, A. B., and Kaul, S., "Handheld ultrasound versus physical examination in patients referred for transthoracic echocardiography for a suspected cardiac condition," *J. Am. Coll. Cardiol. Img.* **7**(10), 983–990 (2014).

[2] Sippel, S., Muruganandan, K., Levine, A., and Shah, S., "Review article: Use of ultrasound in the developing world," *Int. J. Emerg. Med.* **72** (December 2011).

[3] Poland, M. and Wilson, M., "Light weight wireless ultrasound probe." Patent US 2010/0168576 A1 (2010).

[4] Larson, III, J. D., "2-D phased array ultrasound imaging system with distributed phasing." Patent US 5229933 (July 1993).

[5] Savord, B. and Solomon, R., "Fully sampled matrix transducer for real time 3D ultrasonic imaging," in [*Proc. IEEE Ultrason. Symp.*], **1**, 945–953 (2003).

[6] Zhao, K.-Q., Bjåstad, T. G., and Kristofferson, K., "Error analysis of subaperture processing in 1-d ultrasound arrays," *IEEE Trans. Ultrason., Ferroelec., Freq. Contr.* **62**, 663–672 (April 2015).

[7] Siemens Medical Solutions USA, Inc., "Datasheet - ACUSON Freestyle$^{\text{TM}}$ Ultrasound System - Release 3.5," (2014).

[8] Hemmsen, M. C., Kjeldsen, T., Lassen, L., Kjær, C., Tomov, B., Mosegaard, J., and Jensen, J. A., "Implementation of synthetic aperture imaging on a hand-held device," in [*Proc. IEEE Ultrason. Symp.*], 2177–2180 (2014).

[9] Hemmsen, M. C., Lassen, L., Kjeldsen, T., Mosegaard, J., and Jensen, J. A., "Implementation of real-time duplex synthetic aperture ultrasonography," in [*Proc. IEEE Ultrason. Symp.*], 1–4 (2015).

[10] Kortbek, J., Jensen, J. A., and Gammelmark, K. L., "Sequential beamforming for synthetic aperture imaging," *Ultrasonics* **53**(1), 1–16 (2013).

[11] Hemmsen, M., Hansen, P. M., Lange, T., Hansen, J. M., Hansen, K. L., Nielsen, M. B., and Jensen, J. A., "In vivo evaluation of synthetic aperture sequential beamforming," *Ultrasound Med. Biol.* **38**(4), 708–716 (2012).

[12] Jensen, J. A. and Svendsen, N. B., "Calculation of pressure fields from arbitrarily shaped, apodized, and excited ultrasound transducers," *IEEE Trans. Ultrason., Ferroelec., Freq. Contr.* **39**, 262–267 (1992).

[13] Jensen, J. A., "Field: A program for simulating ultrasound systems," *Med. Biol. Eng. Comp.* **10th Nordic-Baltic Conference on Biomedical Imaging, Vol. 4, Supplement 1, Part 1**, 351–353 (1996).

[14] Hansen, J. M., Hemmsen, M. C., and Jensen, J. A., "An object-oriented multi-threaded software beamformation toolbox," in [*Proc. SPIE Med. Imag.*], **7968**, 79680Y 1–9 (March 2011).

[15] Ranganathan, K. and Walker, W. F., "Cystic resolution: A performance metric for ultrasound imaging systems," *IEEE Trans. Ultrason., Ferroelec., Freq. Contr.* **54**(4), 782–792 (2007).